Chapter

Semiconductor Surface State Engineering for THz Nanodevices

Irving Eduardo Cortes-Mestizo, Edgar Briones, Leticia Ithsmel Espinosa-Vega and Victor Hugo Mendez-García

Abstract

This chapter is dedicated to study the semiconductor surface states, which combined with nanolithography techniques could result on remarkable properties of advanced nanodevices suitable for terahertz (THz) signal detection or harvesting. The author presents the use of low-dimensional semiconductor heterostructures for the development of the so-called self-switching diodes (SSDs), studying by simulation tool key parameters in detail such as the shape and size of the two-dimensional electron gas system. The impact of the geometry on the working principle of the nanodevice and the effects on current-voltage behavior will be described in order to acquire design guidelines that may improve the performance of the self-switching diodes when applied to low-power square-law rectifiers as well as elements in rectennas by appropriately setting the size of the components.

Keywords: surface states engineering, self-switching diode, L-shape, V-shape, W-shape, rectenna

1. Introduction

The terahertz frequency range of the electromagnetic spectrum represents a technology gap between the electronic and optical well-stabilized technologies. Thus, the obtention of systems designed to generate, detect, and process THz radiation still is of scientific attention by the full of potential applications. Meanwhile sources available nowadays are typically expensive, fallible, and voluminous. It is possible to extend the electronic and optic concepts, for the THz radiation with millimetric and micrometric wavelength, respectively. However, the use of electronic in the THz range needs small circuits and high-frequency cutoff, while optical requests deal with the dimensions necessaries to work in the THz range [1].

Electronic has been one of the most advanced technologies applied in the modern life, being imperative to extend the electronic concepts such as resistance, diode, and transistor to operate in the THz range with the aim to fill the so-called THz gap by small, efficient, and low-cost technologies. The use of electronic devices in THz implies both high carriers' mobility and short flight time of carriers between electrodes. The nanodevices are one of the most promising alternatives to the development of the THz technology. Recently, the semiconductor nanodevices have been employed for the generation and detection of THz radiation [1–6] showing an enormous potential for their application.

A wide variety of physics phenomena has been used to generate THz radiation by the manipulation of materials systems. THz radiation generation technology can be roughly classified into two categories: photonic and electronic. Phenomena such as the photo-Dember effect [2], Gunn oscillations [3], quantum cascade lasers [4], and difference-frequency mixing in nonlinear crystals [5] have been used to generate THz through the electronic approach. In these techniques, the semiconductor material has a crucial role, and its properties can be further improved by the use of nanostructures. On the other hand, the most applied THz detectors are classified into bolometers and photoconductors. The widely used bolometer is based on temperature variations caused by THz radiation absorption [6].

Important challenges arouse in the development of novel semiconductor nanodevices tuned in THz range to be operated at room temperature (RT). The nanodevice performance at 300 K is reduced principally for the high-impedance nature of this type of technology and the low carrier mobility. In order to improve the RT properties of nanotechnology semiconductor devices, very sophisticate deposition technology has been used where the layer thickness must be controlled as thin as less than one monolayer.

Molecular beam epitaxy (MBE) has been one of the most popular techniques to the fabrication of semiconductor nanostructures used in the development and improvement of nanodevices, achieving faster and efficient electronic and optoelectronic devices like solid-state lasers [7], solar cells [8], and high-electron-mobility transistors (HEMTs) [9]. MBE has allowed the expansion of low-dimensional semiconductor systems, where carriers are restricted to move into two, one, or zero spatial dimensions, becoming an attractive field for researchers due to the possibility to obtain quantum effects that are promisors to fill the so-called THz gap. For example, quantum dots (zero-dimensional restriction) are capable to emit radiation in the THz region as result of their energy states, which depend on its physical dimensions and act as recombination centers for carriers generated in the GaAs layers within the structure when they are exited with a femtosecond optical pump at 800 nm [10]. Additionally, MBE allows for the construction of semiconductor structures with atomically abrupt and flat interfaces that in conjunction with band-structure engineering permit the obtention of high-purity heterostructures embedding a two-dimensional electron gas (2DEG) [11]. In the heterostructures with 2DEG, carriers are confined to a very narrow layer of thickness smaller than De Broglie wavelength which can travel without scattering caused principally by impurities. The large mean free path of electrons in 2DEG is translated into high mobility in the order of 14.4×10^6 cm^2/Vs at low temperature. This high mobility is not possible to be obtained in traditional bulk materials [12].

The use of the modulation-doped semiconductor heterostructures with high-mobility electrons confined to two dimensions in field-effect transistors originated the so-called high-electron-mobility transistor (HEMT). In these devices, the low-temperature mobility was improved over time, leading to innovations in solid-state physics, high frequency, and low-noise electronics [9, 12]. The speed of transistors has been increased over time. HEMTs have demonstrated the highest frequency of operation over 1.5 THz when a combination of techniques such as reducing gate length, material purity, and doping schemes are used in their fabrication [11–13].

High carrier mobility can be proportionated by the appropriate design of modulation-doped heterostructure, where the 2DEG is present. Short flight time of carriers between electrodes is originated by size miniaturization where semiconductor devices enter into the ballistic transport regime, allowing them to be used in high-speed applications. Nevertheless, the current miniaturization technology reaches nanometric dimensions where the extent of surface atoms on

semiconductor materials represents an important percent of the whole device, making the performance of the nanodevices be affected by these outmost atoms. Surface physics plays an important role for the functioning and performance of semiconductor nanodevices, being imperative to understand and predict how surface states, surface charge, and near-surface depletion regions can be manipulated in order to engineer nanoscale devices designed to operate at THz frequencies.

1.1 The semiconductor surface

The characteristics and properties that characterize a semiconductor material such as carrier concentration, band structure, or bandgap result from assuming that translational symmetry of infinite bulk crystal is present in all the material volume. However, when the three-dimensional symmetry in the occurrence of a surface is interrupted, it makes the bulk assumptions inadequate. Therefore, to understand the mode that surface properties can be manipulated to produce nanodevices capable to operate at THz range, it is necessary to understand the different behavior adopted by the surface and the effects over the whole semiconductor characteristics.

The sudden termination of the translational symmetry of the crystal lattice at surface originates surface atoms with unpaired electrons. In **Figure 1(a)** the ideal surface atomic arrange is exhibited. In this case, the topmost atomic bonds of surface atoms acquire the same configuration than bulk atoms, in a perfectly periodic two-dimensional surface. The surface bonds assume that lattice cell keeps repeating such if a virtual lattice is deposited above them. Atoms in an ideal surface present similar properties than those atoms from beneath layers in the bulk structure, exhibiting the condition of flat band, where the conduction band (E_C) and valence band (E_V) have the same energy position contrasted with the bulk region. This state is illustrated in **Figure 1(b)**.

The ideal surface is not usually exhibited in III–V semiconductors because free surface bonds involve excessively high-energy states. Surface bonds use both mechanisms to reduce energy: surface reconstructions and reaction with atoms in the atmosphere, usually oxygen. After, the three-dimensional symmetry of surface lattice is changed in the last nanometers. This condition is schematized in **Figure 2(a)**. Surface reconstruction and surface reactions produce electronic states. These states have no equivalent in the band structure of the bulk crystal. Consequently, in real surface the existence of surface states N_S should be considered, positioned inside the semiconductor bandgap, which generally serve as traps for free carriers.

The presence of N_S, sometimes called midgap states, at surface causes important effects on the carrier's distribution and Fermi-level (E_F) position relative to the E_C

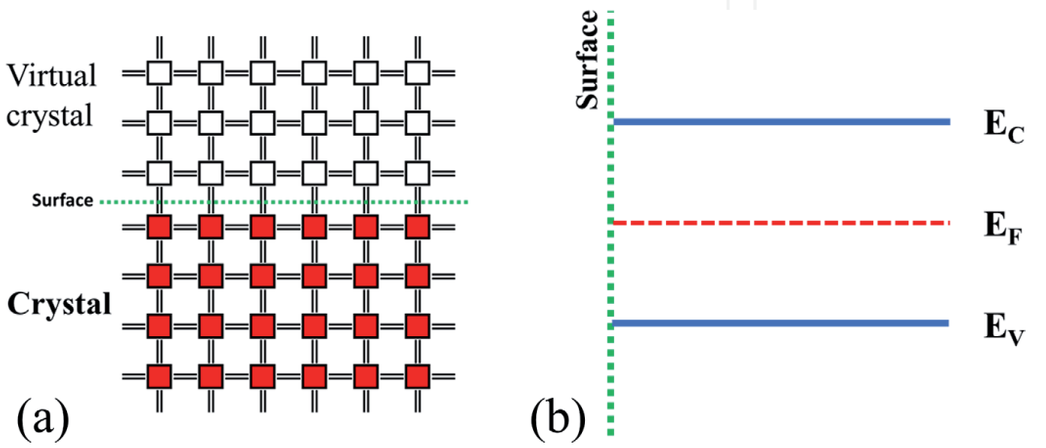

Figure 1.
Ideal surface representation of (a) crystal structure and (b) band diagram.

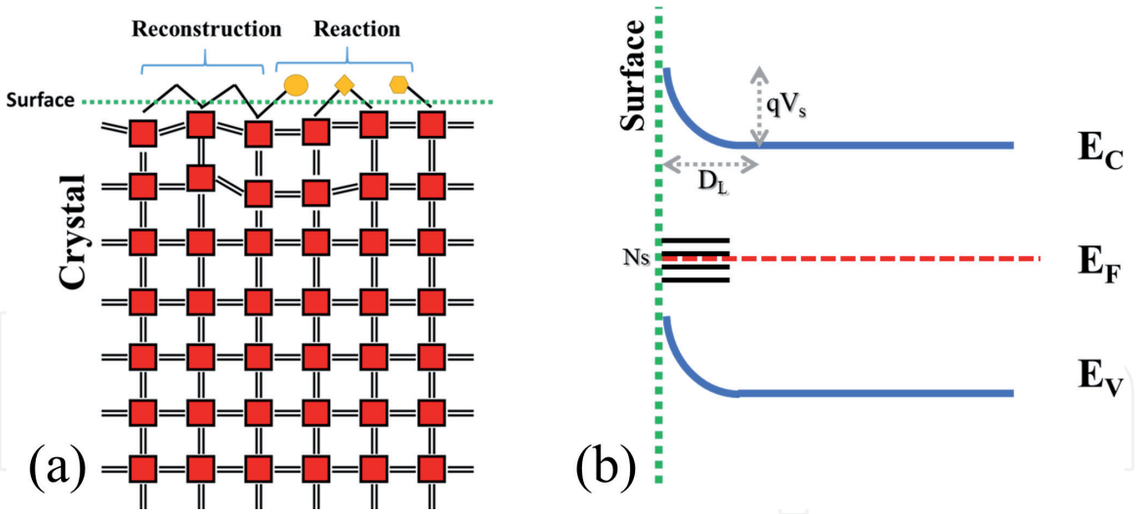

Figure 2.
Real surface representation of (a) crystal structure with surface atom reconstruction and reaction. (b) Band diagram with surface state effect.

and E_V near the surface. The N_S position inside the bandgap offers low energy levels in comparison with E_C and E_V for carriers, and two types of N_S can be recognized according to the charge that is acquired when occupied. Donor-type surface state is obtained when Ns exhibited a positive charge after filled in. On the other hand, acceptor-type surface states are obtained if filled by electrons [14].

In n-type semiconductor, when electrons migrate from their hypothetical bulk positions toward the acceptor-like N_S, two phenomena occur. First, the ionized host atoms lead to the formation of a depletion region, D_L, with a space charge layer. The charge neutrality principle is accomplished when a charge accumulation in a thin region of the surface, n_{SS}, is created by the filling of the N_S. This redistribution of charge is governed by Poisson's equation [15, 16], propitiating the formation of a built-in electric field (E_S) and a voltage (V_S) close to the surface related by

$$V_S = E_S \frac{D_L}{2}. \quad (1)$$

The existence of N_S in the bandgap produces the so-called effects of Fermi-level pinning and the band bending at surface by the formation of a surface barrier with height of $\Phi = qV_S$.

With the purpose to avoid surface effects, a lot of methods have been employed, e.g., altering the chemical composition of the surface modifies the energy of the N_S [16]. It is crucial to recall that band bending is produced by n_{SS} accumulated at semiconductor-environment interface, being possible to modulate the charge density at surface by illumination that would generate electron-hole pairs, which are recombined at surface. Another form to modulate the carrier's population in N_S is by applying an electric field that will exert a selective attraction/repulsion process over the carriers. Accordingly, in surface state engineering, it is imperative to understand and predict how N_S, n_{SS}, and D_L can be manipulated in order to engineer nanoscale devices capable to operate in the THz region.

2. The self-switching diode

The THz systems for detection are roughly divided into two groups according to the detection of amplitude and phase (coherent heterodyne systems) or only amplitude of the signal (noncoherent forward detection systems). The most applied

THz detectors are the bolometers, Schottky barrier diodes, pair-braking detectors, hot electron mixers, and field-effect transistors [17]. Special interest in detector lies in the diode concept, since it is one of the more useful components in electronic engineering, allowing current flow only in one direction.

The diode concept has a very large variety of applications that stimulate the application of semiconductors in electronics. Nevertheless, the cut-off frequency is still under improvements today. For THz detection, ultrafast metal-insulator-metal (MIM) and metal-insulator-insulator-metal (MIIM) tunnel barriers or p-n semiconductor junctions (reverse Esaki tunnel diodes) have been used [18, 19]. Nonetheless, they show low rectification capacity due to their poor diode-like behavior.

One alternative to get a diode device able to operate in the THz regimen is the self-switching diode (SSD) which was first proposed and developed by Song [20]; this device is schematized in **Figure 3(a)**. The properties and performance of the SSD are dependent on both the characteristics of the heterostructure and the grooves etched on it. First, the two-dimensional electron gas (2DEG) created in the heterostructure and illustrated in **Figure 3(b)** is the core of the SSD device, and it is possible to increase the mobility by an adequate layer sequence design. The modulation-doped heterostructures are an excellent example of the importance of the 2DEG properties, since they lead to the development of the high-mobility devices such as the HEMT. The second important element in the SSD structure is the insulating grooves, which can be realized by standard electron beam lithography and wet etching [20].

Due to the groove fabrication process, the symmetry of the crystal structure in the trenches wall is broken, creating N_S. The filling process of N_S produces the formation of a lateral n_{SS} in the trench walls and therefore a D_L inside the nanochannel. The working principle of the SSD is the modulation of the lateral n_{SS} by the bias applied in the ohmic contacts of the device. The current only flows when the anode contact has a positive voltage value with respect to the cathode contact and the grooves force the current to flux only by the nanochannel. In the SSD fabrication process, only one step of lithography is necessary, reducing the cost of production and the use of complex mask alignment steeps [21].

The SSD device has been demonstrated using heterostructures where the 2DEG is presented such as systems based on InAlAs/InGaAs and AlGaAs/GaAs multilayer structures [21, 22]. The working principle of the device is not dependent on the 2DEG properties, allowing to be fabricated in bulk materials like silicon [23] and transparent semiconductors like ZnO and indium tin oxide (ITO) [24, 25], and graphene-based SSD has been also demonstrated [26]. Those devices have exhibited

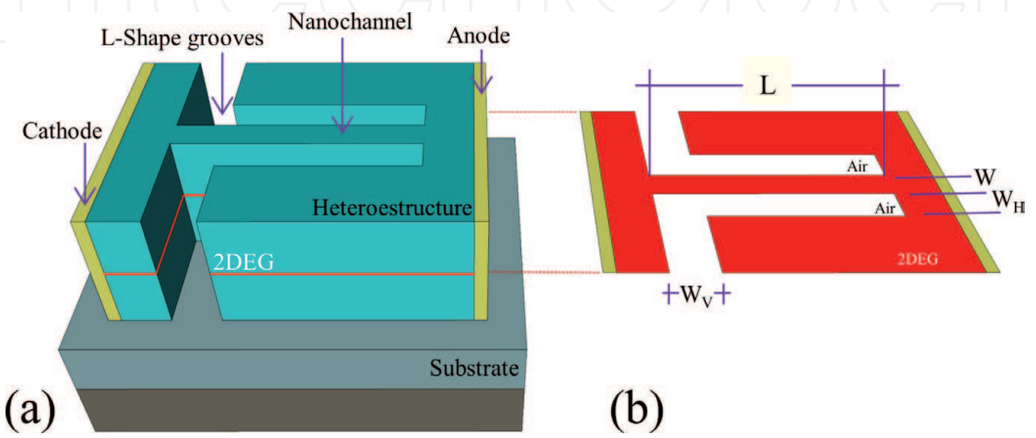

Figure 3.

(a) Self-switching diode layout structure, based on a 2DEG-containing heterostructure. (b) Top view of two-dimensional SSD L-shape topology. The parameters and the nomenclature to define the L-shape SSD geometry are channel length L, channel width W, vertical W_V, and horizontal W_H groove thickness.

the ability to detect extremely weak signals without applied bias [27, 28]; their high sensitivity [29] and their capability to operate in the terahertz regime [27, 30] make the SSD concept a rewarding tool that has opened a broad range of applications that support the THz gap filling.

2.1 Simulation analysis details

The SSD schematized in **Figure 3** represents a real device where it is appreciated that basically the SSD is made with two L-shape grooves etched on a heterostructure with a 2DEG. Hence, it is possible to analyze the SSD performance from two points of view: the heterostructure (one-dimensional) and the groove (two-dimensional) geometry in order to avoid three-dimensional numerical analysis required to simulate the electrical behavior of the SSD device.

The heterostructure component of the SSD can be modeled by Schrödinger-Poisson equation, considering the material and layer sequence in order to get the band profile and calculate the electron distribution in the samples [16]. This type of analysis is useful to determinate the properties of a 2DEG in the heterostructure, which gives the carriers high mobility required to operate in THz. **Figure 4(a)** shows the layer sequence of an InGaAs-/InAlAs-based heterostructure, for which the SSD concept has been experimentally proved [20]. The sequence, material, and thickness of each layer are used as input parameters of the 1D model, else the delta doping (δ-doping) concentration.

Figure 4(b) exhibits the 1D simulation output; the profile of the conduction band of the heterostructure of **Figure 4(a)** is plotted. As observed in the simulation, at the interface InGaAs/InAlAs, the E_C bends toward energies under the Fermi level producing a triangular quantum well with one allowed energy state (E_1). When electrons populate the E_1 sub-level, electrons can move freely along two dimensions. Thus, the electrons are confined within a 2D sheet embedded in a 3D heterostructure. High concentration and high mobility are exhibited by the electrons trapped in the triangular quantum well, making the heterostructure suitable for THz devices.

With the aim of determining the SSD current-voltage behavior (I-V), we employed a commercial physically based device simulator in two-dimensional mode, similar to that reported for 2DEG-based InGaAs SSD and silicon-on-insulator structures [23, 30, 31]. In this model, only the 2DEG layer geometry resulted after the lithography process is analyzed. This type of numerical analysis requires a 2DEG input, where the top view of the SSD and electrical properties of

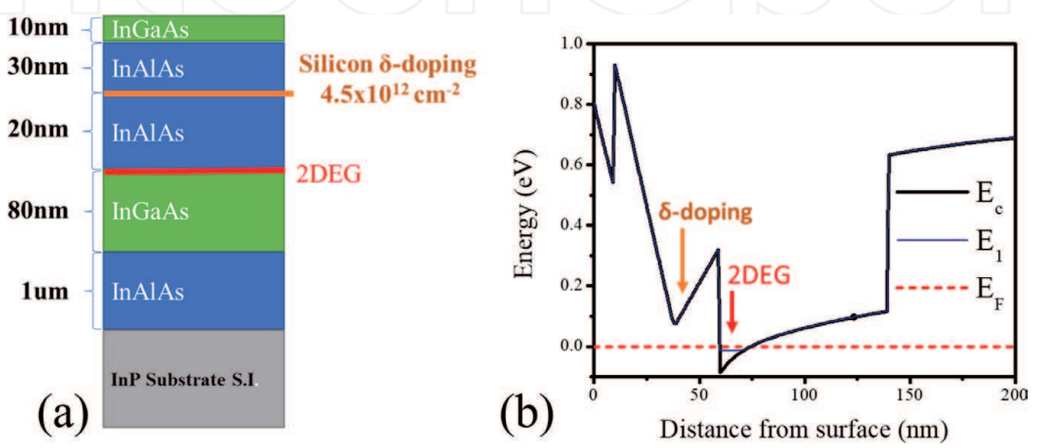

Figure 4.
(a) Layer sequence of the heterostructure analyzed in this work [20]. (b) 1D analysis of conduction band edge energy diagram of the structure at room temperature. The red line indicates Fermi-level position.

the 2DEG are considered as simulation inputs. The SSD layout of **Figure 3(b)** is the schematic top view of an L-shape SSD, showing the geometrical frameworks used in the simulation. The electrodes shown in **Figure 3** have been labeled as anode and cathode according to the convention that in the ideal diode, the carriers flow from anode to cathode.

The background doping and the electron mobility of the 2DEG samples utilized in the simulation were 1×10^{17} cm^{-3} and 12,000 cm^2 V^{-1} s^{-1}, respectively, under no impurity scattering. The dielectric material filling the grooves was air ($\varepsilon_r = 1$), inducing a surface charge density of $n_{SS} = 0.4 \times 10^{12}$ cm^{-2}. The contact resistivity used in the simulation process was 1×10^{-8} Ω cm^2, which is similar to standards that exist for THz devices [32]. Finally, the energy balance model at 300 K was used. The model was employed to perform a systematic geometrical analysis and comparing different types of self-switching structures directed to provide an enabling technology for energy harvesting in the terahertz region. Since the self-switching diodes combine size and electronic transport property effects, the performance of different SSD was analyzed and optimized by changing their shape configuration.

2.2 Self-switching diode working principle

The key to understand the DC performance of the SSD lies on the modulation of the n_{ss} inside the N_S by the built-in electric field, producing a modification in the D_L along the nanochannel. In this way, some authors indicate that the SSD can be understood as a two-dimensional field-effect transistor with gate and drain short circuited where flanges act as a double lateral-gate terminal [28, 33]. The principal mechanism that controls the carrier transport of the SSD is explained in terms of the free carriers that can participate in conduction phenomena and travel through the nanochannel [22]. To expose the SSD performance and their rectifying nature, it is necessary to explore the L-shape device shown in **Figure 5(a)** used as simulation input parameter and termed as the reference geometry. The result of the numerical study is the electron-charge distribution along the 2DEG plane illustrated in **Figure 5(b)** when both electrodes are unbiased.

With no applied bias, simulations show a drastic reduction of the background carrier density inside the nanochannel as a consequence of the electron filling of the N_S created at groove walls. Carrier density decays from the background rate (1×10^{17} cm^{-3}, in orange-red color) to 10^{14} cm^{-3} (cyan color) along the length of the nanochannel and decreases steadily closer to the groove walls, remaining

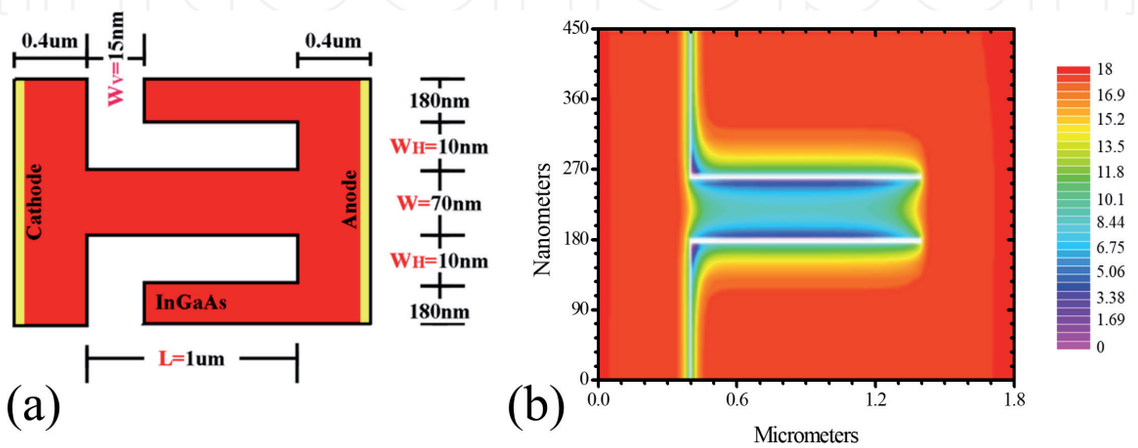

Figure 5.
(a) Top view schematic representation of the proposed L-shape self-switching nanochannels. (b) Electron charge distribution along the 2DEG plane inside the nanostructures under zero bias.

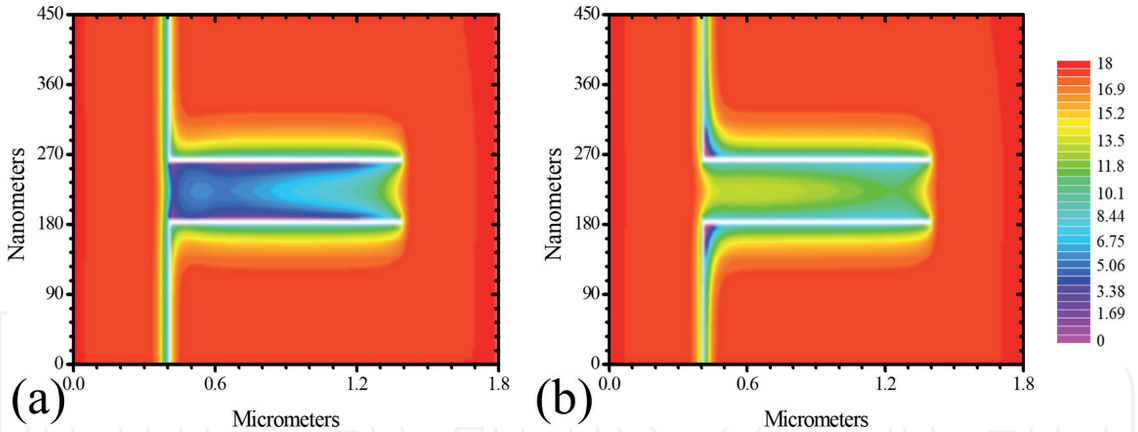

Figure 6.
Electron density distribution (logarithmic scale) for the SSD with the geometry depicted in **Figure 5(a)** *at (a) V = −0.5 (reverse bias) and (b) V = 0.5 (forward condition).*

homogenous all along the L-shape channel, as it is displayed by **Figure 6(b)**. In other words, the D_L created inside the nanochannel limits the free carriers available to participate in conduction phenomena defining high-resistive or not conductive nanochannel.

For reverse bias (V = −0.5 V in the anode, while cathode is set to ground), the charge depletion effects are enhanced along the channel due to the transversal electric field that appears at the groove walls, lowering the carrier density inside channels, according to **Figure 6(a)**. For reverse state, the D_L inside the nanochannel is raised by two orders of magnitude in comparison with the zero-bias case, making a pinch-off condition that prevents any current to flow along the nanochannel due to the lack of carriers. However, reverse current can be established when the bias is high enough to overcome the lateral depletion effects.

Figure 6(b) displays the carrier distribution at V = +0.5 V for the reference L-shape SSD as forward bias which is settled when a positive voltage is applied to the anode. Under forward polarization the n_{SS} in the N_S of the SSD trenches is deflated, reducing the D_L inside the nanochannel. On this condition, the carrier density increases several orders of magnitude ($\sim 10^{15}$ cm^{-3}), close to the background concentration when the D_L is reduced by the transversal electric field. The electron transport along the channel is possible at this condition by the intensifications of the free carrier concentration.

The analysis of the carrier distribution along the 2DEG, where the SSD has been fabricated in addition with the extension/modulation of the D_L inside the nanochannel, indicates that it is possible to control the current flux that travels between electrodes by controlling the free carrier inside the nanochannel. This modulation is originated by the sign of the applied voltage in the anode, making the SSD a rectifier element capable to operate in the THz region by the high-mobility nature of the 2DEG of the heterostructure where the nanometric dimensions of the L-shape grooves are lithographed.

In DC injection mode, the performance of a rectifier element can be simply analyzed by the nonlinearity of their current-voltage curve, the threshold voltage (V_{TH}), and the leakage current present in reverse bias. These properties can be examined by the D_L width inside the nanochannel. The zero-bias simulations indicate that there is a minimum carrier concentration, which propitiates the formation of the D_L necessary to be modulated by the applied bias, being dependent of the groove fabrication process and the nanochannel shape, especially.

Therefore, in the SSD initial design, it is mandatory to achieve a nanochannel with the appropriated carrier concentration at 0 V. As it is going to be analyzed

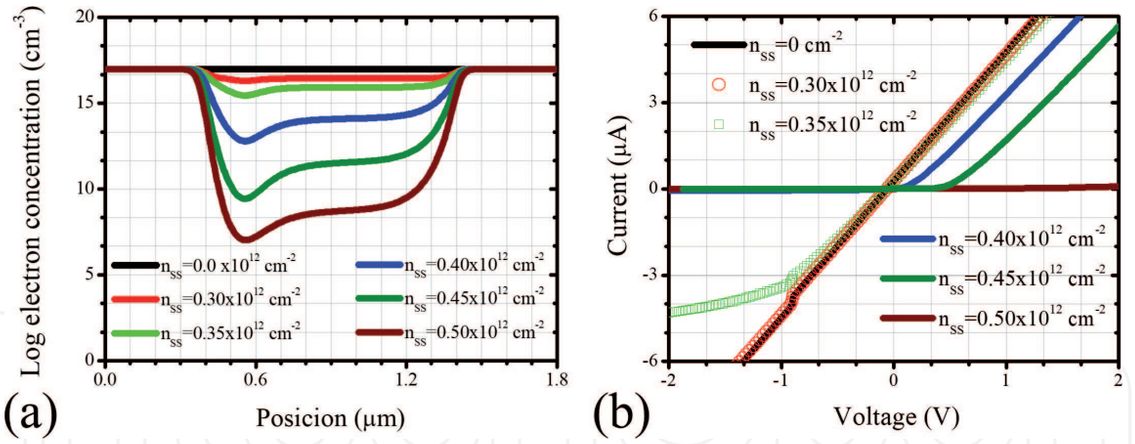

Figure 7.
The effect of the surface charge density (n_{SS}) on (a) the electron concentration along the device and in (b) the current-voltage characteristics.

in the following sections, the nanochannel shape, width, and length ensure that the SSD exhibits diode-like behavior and would provide an estimation of the V_{TH} necessary to turn on the conduction of the SSD. Nevertheless, the N_S are difficult to control in a desire range though they can vary considerably depending on the L-shape groove fabrication techniques such as etching methods, leading to crucial effects on the DC and AC performance of the SSD device.

According to surface physics, the n_{SS} agglomerated in the interface semiconductor environment is a manifestation of N_S. The SSD fabrication determines the available surface states. When the device processing augments the N_S density, more electrons will be used to fill these states, magnifying the D_L inside the nanochannel. Therefore, the rise (reduction) of the n_{SS} has the effect to decrease (increase) the free carriers' density along the channel. **Figure 7(a)** exhibits the carrier distribution along the SSD device from the nanochannel calculated at 0 V when the n_{SS} was varied from 0 to 0.5×10^{12} cm^{-2}. It is clear to see that for the $n_{SS} = 0$, there is not a modification in the free electron concentration along the channel, declining considerably for $n_{SS} > 0.35 \times 10^{12}$ cm^{-2} and enhancing as n_{SS} increases.

Hence, the carrier density inside the nanochannel and their modulation are used to propitiate the rectifier behavior of the SSD device. The current-voltage curve of the SSD-based structure ($n_{SS} = 0.4 \times 10^{12}$ cm^{-2}) is exhibited in **Figure 7(b)** where the diode typical I-V curve is presented. In the case of $n_{SS} = 0$, the I-V is completely lineal; in other words, the absence of N_S produces that the SSD works like a resistor device. When the $n_{SS} = 0.35 \times 10^{12}$ cm^{-2}, the nonlinearity of the I-V curve is exhibited, with a V_{TH} near to zero, a desired value for low-power signal detection. Nevertheless, in this case the reverse bias exhibits an important leakage current. For $n_{SS} > 0.35 \times 10^{12}$ cm^{-2}, the reverse current is removed notoriously, improving the diode-like performance, while an excessive n_{SS} steps the V_{TH} up, improving the nonlinearity and avoiding leakage current.

According to the simulation results, carrier density exhibited by the non-polarized structure indicates that a minimum bias, or voltage threshold, is required in order to propitiate electron conduction. In that case, the lower the carrier concentration is, the higher the V_{TH} results. For short D_L length, low bias is required to turn the SSD on; nevertheless, an important leakage current is present. By modulating the dimensions of the depletion region inside the nanochannel, the L-shape SSDs are found to be suitable for detection of very weak signals, making the SSD concept an important tool in the development of high-frequency integrated circuits since it has been demonstrated that by choosing appropriate geometrical dimensions, the rectification efficiency can be optimized [33, 34].

3. Self-switching diode design guidelines

In order to get a rectifier with cut-off in the THz region by the SSD device, it is important to follow design considerations that may improve the current rectification with low V_{TH} and optimize the SSD up for the best efficiency. These considerations are related to the geometry-depletion region relationship between the SSD dimensions, shape, and the D_L extension. In this section, we evaluate the rectification performance of the L-shape SSD device in DC injection mode by a systematic analysis where the width, W; the length, L; and the vertical and horizontal trench width (W_V and W_H) of the channels are varied in order to get their effect on the I-V behavior of the device. The layout shown in **Figure 5(a)** defines the reference geometries where we have a varied chosen parameter, while the others were fixed.

The simulations were carried out in order to obtain the I-V curves of each geometrical variation with the aim to evaluate the ability of channels to detect the electrical energy of low-voltage THz signals. On this way, the SSDs can be considered as square-law rectifiers that generate electrical power from the incoming THz radiation. In order to understand the size effect on the detection, we use three criteria that define the performance of the SSD. Fist, differential resistance, R_V, of the SSD can be found using the I-V response, key issue for determining the impedance matching between the channels and the signal acquisition system, and it is defined by

$$R_V = \left(\left. \frac{dI}{dV} \right|_{V=0} \right)^{-1} \tag{2}$$

The nonlinearity (N_V), which expresses the diode-like I-V curve behavior, can be determined by evaluating

$$N_V = \left. \frac{d^2 I}{d V^2} \right|_{V=0}. \tag{3}$$

N_V is a main issue for the performance of the rectifier because of higher nonlinearity result in a larger DC output. The impact of R_V and N_V is resumed in the sensitivity, γ_0, of the device, which is calculated by $\gamma_0 = N_V R_V$. R_V, N_V, and γ_0 are usually studied at zero bias, heeding the fact that detection must be performed with no feed bias [35].

3.1 Geometry dimension impact on I-V characteristics

In **Figure 8(a)** the effect of modification in the channel width (W) through I-V curves is presented. It is observed that when W is widened, V_{TH} is reduced as a consequence of the spatial restriction of the electrons that could occupy the surface states inside the grooves in order to maintain charge neutrality. Large D_L indicates high diode resistance and requires high voltage in order to deplete or drain the surface states, producing that R_V goes from 143 MΩ to 233 kΩ when W is broadened from 60 to 80 nm, respectively.

According to Ohm's law, the current is improved as the thickness W is widened by the reduction of R_V. Therefore, by the design of the channel width, it is possible to control the SSD's worth V_{TH} and R_V. Nevertheless, large W generates reverse current at low negative bias, and, as a result, the diode-like character disappears lowering γ_0. Therefore, in order to avoid a reverse current flow and design for a low-threshold voltage V_{TH} device, it is necessary to consider the relationship between the surface charge and W [22, 30].

Figure 8(b) shows I-V characteristics of SSDs with several channel lengths, L, where it is appreciated that V_{TH} shifts to lower voltages when L is reduced due to the

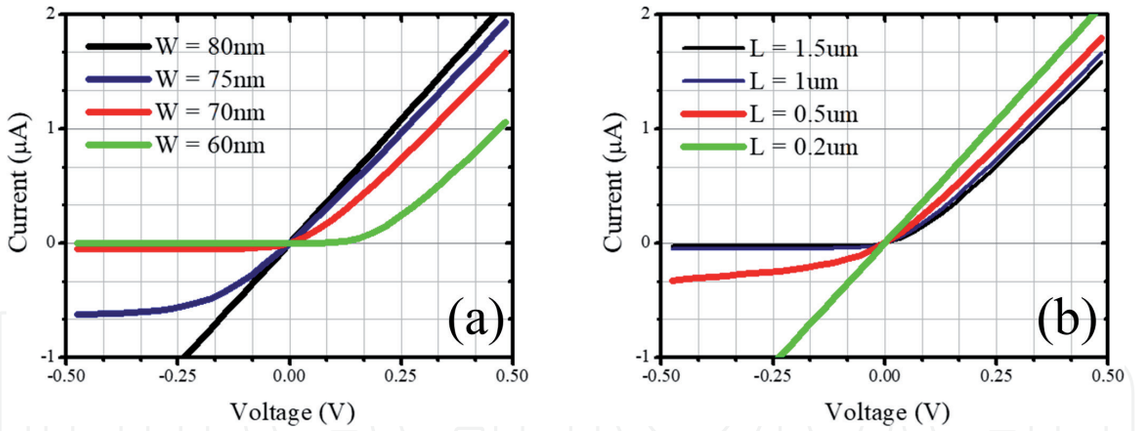

Figure 8.
Current-voltage behavior of the L-shape SSD-based geometry when (a) the channel width (W) parameters are varied from 60 to 80 nm and (b) the channel length (L) is modified from 0.2 to 1.5 μm.

decrease in D_L inside the nanochannel. Small D_L length facilitates ballistic transport; in the meantime that carrier's mean free path is larger than the D_L and reduces R_V. For this case, when L is reduced from 1.5 to 0.5 μm induces a change on R_V from 1.3 MΩ to 423 kΩ. Nevertheless, the reduction of D_L through the reduction of L favors the presence of an important leakage current for reverse bias, affecting the I-V nonlinearity and inducing a reduction in the sensitivity of the devices.

Therefore, for 2DEG-based SSD intended to work at THz frequencies, it is necessary to reduce the carrier's time of flight between electrodes, which can be achieved by improving the electron mobility of the 2DEG, the carrier's mean free path getting better or shortening the L extension, considering that at THz frequencies the electron transport is in the ballistic regime [30]. To design a cost-effective SSD THz device, the election of the appropriated length L for the working frequency in function of the 2DEG mobility is mandatory, keeping γ_0 as high as possible.

The impact of the geometrical dimensions on the I-V characteristic of the SSD was performed by the numeric analysis for all geometric parameters indicated in **Figure 5(a)**, and it is resumed by the nominal sensitivity of the SSD in **Figure 9(a)**. For example, the reduction of the W thickness increases the magnitude R_V while weakens the rectifier performance of the SSD by the apparition of an important leakage current, indicating that the N_V is reduced with this modification. The γ_0 reaches 37 V^{-1} for the narrower W of 60 nm, being reduced for wider W. On the other hand, the largest nanochannel length (L = 1.5 μm) originates that γ_0 = 25 V^{-1}, and conversely the sensitivity is reduced by the reduction of the nanochannel length, rendered in **Figure 9(a)**.

The reduction of D_L width and length is not the only mechanism to modify the DC performance of the SSD. Controlling the magnitude of the electric field that modulates electrons in the N_s would have the effect of improving the I-V behavior. In this task, both the vertical and horizontal width trenches (W_V and W_H, respectively) are the main geometrical elements that can be used to achieve modulation of surface states. It was found that W_V in the range of 5–50 nm did not affect the I-V performance of the SSD and consequentially the γ_0 is constant for these modifications and being reduced with W_V > 50 nm. On the other hand, small changes in W_H affected strongly the DC performance of the SSD; meanwhile variation of W_H from 5 to 30 nm resulted in a variation of V_{TH} from 0 to 0.2 V [33, 34], and γ_0 is optimized for W_H = 30 nm. The effect of W_V and W_H trenches is seen in **Figure 9(a)**.

The SSD ability to rectify signals in the THz region relies in the γ_0 value, which can be improved for nanochannel geometry that exhibits long and wide D_L, amplifying R_V and N_V. Nevertheless, narrow W and large L sizes imply to enlarge the V_{TH}.

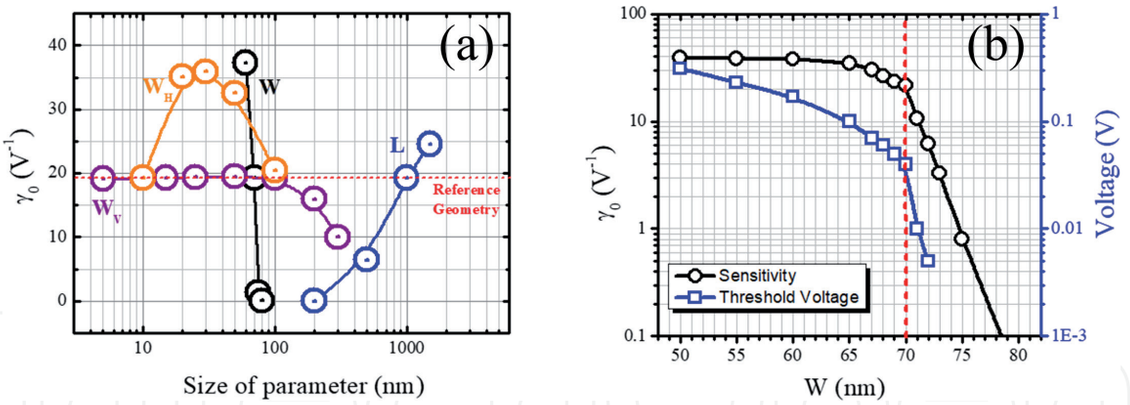

Figure 9.
(a) Sensitivity of the L-shape SSD devices as a function of the size of the geometrical parameters. (b) Effect of modification of W in the V_{TH} and γ_o.

The low-power THz radiation detection needs a rectifier with a threshold voltage close to zero, and according to the simulations, the channel width is the element that strongly defined the γ_0 and V_{TH} performance of an L-shape SSD. Numerical simulations were carried out modifying the W to explore the dependence of γ_0 and V_{TH} with the aim to determine the dimensions of W that propitiate $\gamma_0 > 20\ V^{-1}$ y $V_{TH} < 50$ mV (see **Figure 9(b)**). These desirable conditions are stablished in order to overcome the current performance of the best MIM-tunnel barriers, which exhibit sensitivities between 2.5 and 4 V^{-1} [36, 37].

According to the graph in **Figure 9(b)**, it is possible to obtain $\gamma_0 > 20\ V^{-1}$ for $W \leq 70$ nm, improving the rectifier performance of the SSD. On the other hand, when $W < 70$ nm, the V_{TH} is higher. The best configuration is labeled by the dotted red line at $W = 70$ nm. For $W < 70$ nm, the sensitivity of the SSD is improved, expanding the voltage necessary to turn on the device. Conversely, for W values at the right hand of the dotted red line, the threshold voltage necessary to produce a conductive nanochannel is cut down in the same way with that of γ_0. In other words, the geometrical design of the SSD must consider the application where the SSD is going to be used. The design should consider the power of the signal to be detected in order to choose the tolerance margin between γ_0 and V_{TH} that improves the performance of the SSD.

Rendering to numerical results, the SSD devices combine geometrical effects with the 2DEG properties to act like a rectifier, the nanochannel and trench width in conjunction with the appropriate choice of channel length being key parameters. The optimization of W, W_H, and L induces that the nominal sensitivity of the devices raised to measurement around 40 V^{-1}. Self-switching diodes are good candidates for zero-bias detection and harvesting applications as square-law rectifier elements in the rectenna concept. Nevertheless, the high-impedance nature of the SSD will introduce drawbacks that limit the power transfer between the rectifier and the antenna as it will be shown in the next section.

3.2 Rectennas based on self-switching diodes for THz detection

When the L-shape SSD has been optimized to obtain the best rectifier performance, it is possible to use the device in the detection or harvesting of THz electromagnetic signals. In order to evaluate the efficiency of the SSD as rectifier element in the rectenna concept, we analyze the SSDs coupling to gold-made Archimedean spiral antenna lying on the surface of a semi-infinite SiO_2 substrate and designed to operate between 0.25 and 2 THz with a right-hand circular polarization [38]. **Figure 10(a)** illustrates this antenna design. The simulated performance of the designed micrometric

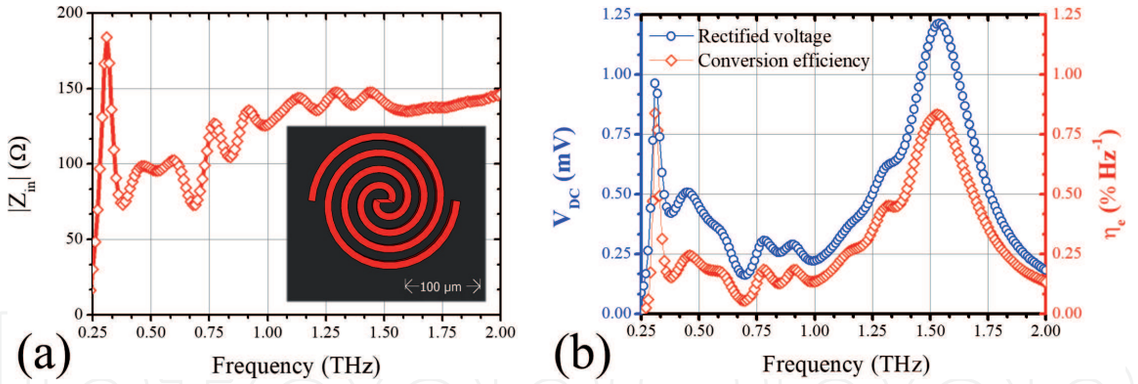

Figure 10.
Performance of L-shape SSD-based rectenna to harvest the optical energy of a terahertz source obtained by the simulation process. (a) Input impedance. Inset shows the Archimedean spiral antenna. (b) Rectified voltage and optical-to-electrical conversion efficiency.

antenna was obtained when it is excited with monochromatic plane waves with an irradiance of 1 W/cm^2 [39] incoming from a precisely tuned terahertz laser. In **Figure 10(a)** the antenna impedance, Z_{in}, is plotted as a first result. In this numeric analysis, we assume that the cut-off frequencies reported for high mobility structures SSD are around 5 THz [22].

The DC voltage generated from the received terahertz radiation by the SSD rectenna is illustrated in **Figure 10(b)**, where a full width at half-maximum parameter of more than 1.8 THz is exhibited with a maximum voltage obtained of 1.25 mV at 1.5 THz. The conversion efficiency of the rectennas is also shown in **Figure 10(b)** as a function of frequency where the total efficiency is found to be ~0.032%. This numerical analysis indicates that in this configuration, the use of L-shape SSDs as rectifiers instead of MIM nanometer diodes enhances the efficiency of the rectennas by a factor of 10^6 [38]. Rectennas based on SSDs are more efficient than those based on MIM barriers due to their I-V characteristic curves, which are more asymmetrical. The relatively low efficiencies (~10^{-2}%) obtained by this SSD rectenna is accredited to the mismatch impedance between the rectifier and the antenna.

From **Figure 10** it is clear that the major voltage and efficiency of the rectenna are obtained when the Z_{in} is raised to about 125 Ω. Higher antenna impedance means a better electrical coupling between the antennas and the diode and more efficient transfer of energy between antenna and rectifier [38]. The coefficient of reflection between both elements is defined by

$$\Gamma = \frac{R_V - Z_{in}}{R_V + Z_{in}}, \tag{4}$$

which exhibits a value around 99.96% for the rectenna system analyzed in this work. In other words, the high magnitude of Γ indicates that only 0.04% of the optical energy is transmitted from the spiral antenna to the L-shape SSD and the rest of the optical power is returned to the spirals [38].

The SSD device performance as rectifier element is modified under unmatched conditions, making necessary to study the R_V behavior on Γ. We use a reference source with a Z_{in} = 50 Ω in order to define the effective sensitivity ($\gamma_{50\Omega}$) to considerer the effects of the unmatched source through the relationship [28]:

$$\gamma_{50\Omega} = \gamma_0(1 - |\Gamma|^2), \tag{5}$$

where Γ is calculated using the Z_{in} = 50 Ω. The $\gamma_{50\Omega}$ criteria describe the performance of the SSD when their electrodes are short circuited to the antenna arms.

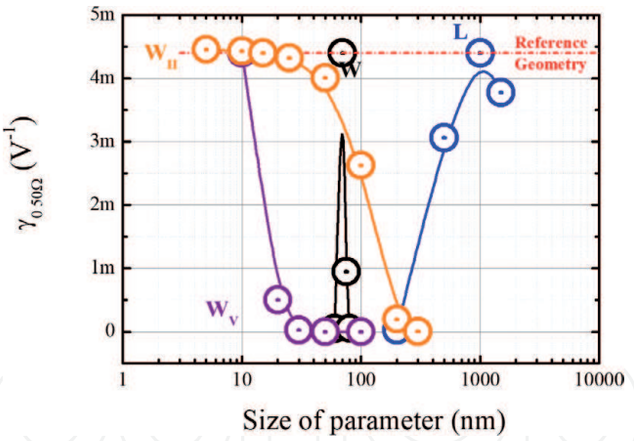

Figure 11.
Effect of the modification of the SSD reference geometry parameters on the effective sensitivity $\gamma_{50\Omega}$.

The trade-off between $\gamma_{50\Omega}$ and R_V is depending on the geometrical parameters; this relationship is illustrated in **Figure 11**.

The numerical results illustrated in **Figure 11** have shown that the reference geometry is the best configuration possible even with the high Γ when they are plugged to a Z_{in} = 50 Ω drive source. This confirms that even when the narrower channels are more sensitive than other structures, they are not the best option to generate and transmit DC electrical power thanks to the high value R_V which heightens the Γ, reducing the power transfer between the antenna and the rectifier. This study indicates that those parameters of the channels that would propitiate to reach higher sensitivities γ_0 are the same with that which produces high $\gamma_{50\Omega}$: the nanochannel width (W), length (L), and the thickness of W_V.

The SSD as square-law detector or rectifier element in energy harvester systems represents an interest alternative, improving the performance of the rectennas based on MIM tunnel barriers, which exhibit very low efficiencies and reduce the technological process required for the rectennas' manufacture, involving only one step of high-resolution lithography. However, to produce terahertz rectennas useful for energy-harvesting applications, an efficient strategy to better match the impedance of the spiral antennas and the self-switching nanodiodes should be incorporated.

4. Self-switching diode shape variations

According to the rectenna performance, a key issue that reduces the use of the self-switching diodes in detection or harvesting applications concerns their high resistance by the nanometric nature of this device. The impedance matching is very difficult, and the losses of the electrical power by reflection will be predominant. The SSD geometry plays the fundamental role defining the DC performance of the device, the design process being a trade-off between geometrical dimensions that exhibits low reverse current in a nonlinear I-V curve with a V_{TH} close to 0 V and, at same time, low channel resistance in conjunction with a high sensitivity quantity. In this section we explore three different SSD shapes to improve their performance as low-power THz rectifier.

The first method to intensify the performance of the SSD is to raise the rectification efficiency by augmenting the numbers of paths through which the carriers travel. In this task, **Figure 12(a)** shows the schematic array of four L-shape SSDs, connected in parallel with geometrical dimensions based on the single SSD of **Figure 5(a)**. The numerical analyses of arrangement for 1, 2, 4, 8, and 16 single

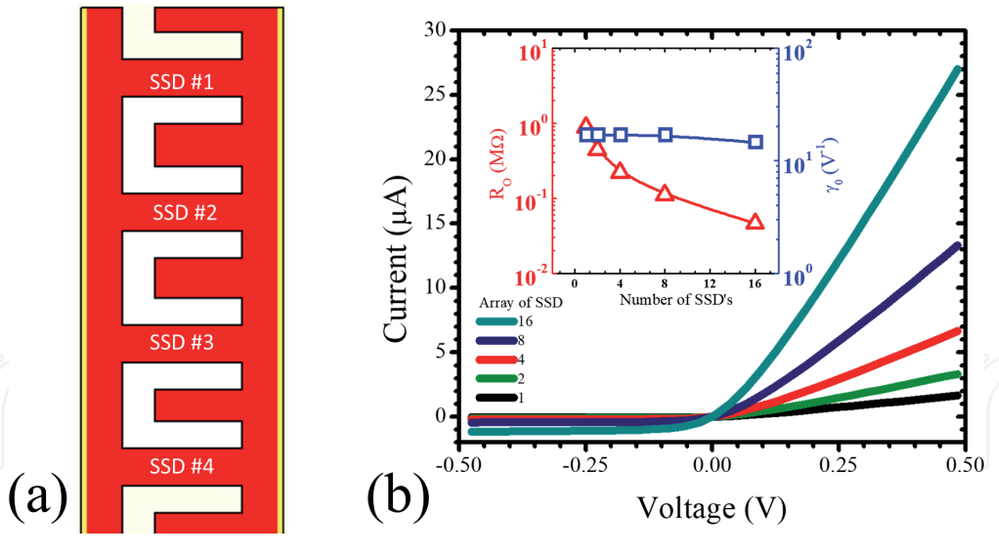

Figure 12.
(a) Top view layout of four L-shape SSDs in parallel array. (b) I-V characteristics of parallel coupled SSD arrangements. The inset shows the R_o and γ_o as functions of the number of SSD elements.

SSDs placed in parallel are exhibited in **Figure 12(b)**. The I-V behavior of the SSD arrays exhibits a small gain of leakage current, while they show threshold voltage of ~0 V. The current is incremented from 1.72 (single SSD) to 28 μA (16 SSD array), representing 16 times larger current in parallel than for a single SSD when the SSD system is biased at 0.5 V.

The augment of SSD elements present in the arrays is translated into a better performance in the current behavior, generating a reduction in the overall resistance, R_O, of the array-based SSD. The changes in device resistance could be considered as $R_O = R_V/N$, where R_V refers to the resistance of the single L-shape element as it is shown in the inset of **Figure 12**. Accordingly, the effect of increasing the number of nanochannels produces R_o changes from 87 to 41 kΩ for a single SSD and 16 SSD arrays, respectively. This reduction in the nanochannel resistance is translated into a reduction in the γ_0 of ~25% as it is plotted in the inset of **Figure 11**. Contrarily, the $\gamma_{50\Omega}$ exhibits a modification from 4×10^{-3} for a single base SSD to 63×10^{-3} V^{-1} for a 16 array-based SSD [33]. It is clear that the major quantity of SSD in parallel results in the reduction of the device resistance, which improves the impedance matching between rectifier elements and antennas by using the appropriate number of SSD [40].

Figure 13(a) exhibits the top view and carrier's distribution for the termed V-shape SSD. In this case, the shapes of the grooves have been modified to reduce the extension of D_L inside the nanochannel by expanding the channel area with the aim to reduce the R_V of the SSD device. According to the SSD working principle, the formation of the D_L along the nanochannel defines the I-V performance of the device. The structure of **Figure 13(a)** and the 2DEG properties described in Section 2.1 were used as input parameters in numerical simulations to analyze the carrier concentration along the V-shape SSD.

When no bias is applied, simulations in **Figure 13(b)** show a drastic reduction of the background carrier density with a width-dependent spatial charge distribution in this shape where electron concentration diminishes close to the channel vortex, reaching populations as low as 6.3×10^{12} cm^{-3} with effective width of 50 nm in a localized region. Reverse polarization is established for V = −0.5 V in **Figure 13(c)**. The pinch-off condition does not occur at −0.5 V occasioned by the small D_L along the channel length, contrasting to the case of the L-shape geometry. Therefore, the carrier distribution can be easily modified to allow the current to flow even at a low reverse bias because of the nanochannel receiving similar carrier concentration for

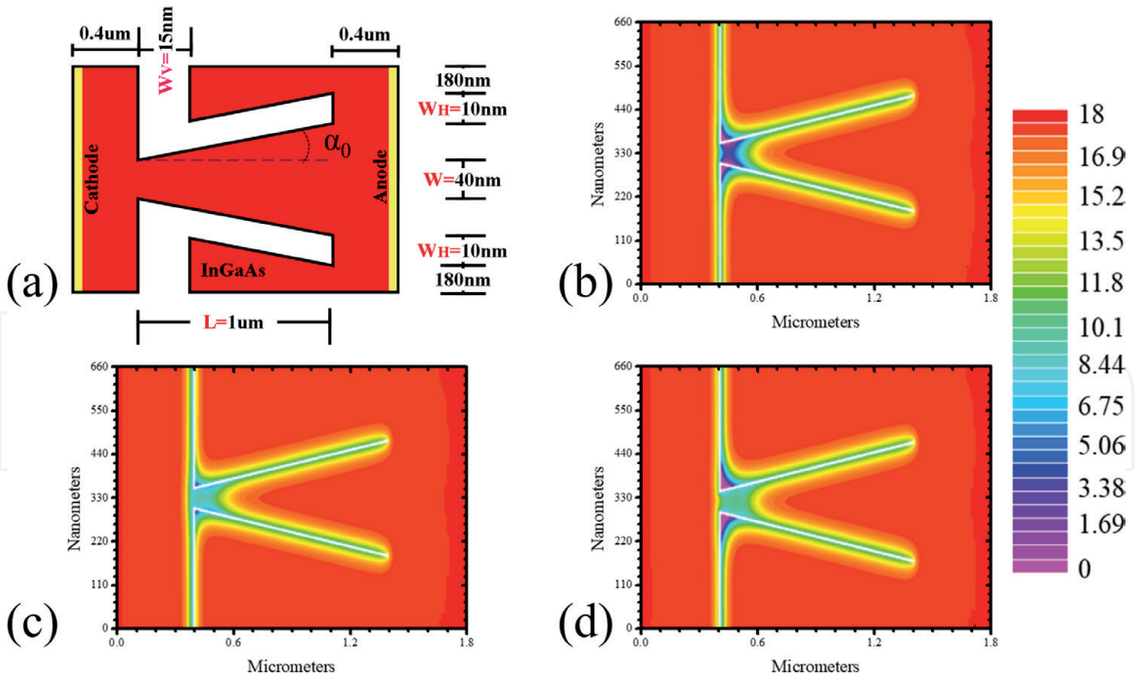

Figure 13.
(a) Schematic representation of the V-shape self-switching diode. Electron charge distribution along the 2DEG plane under (b) zero, (c) reverse (V = −0.5 V), and (d) forward (V = +0.5 V) voltage bias.

reverse and forward condition (at 0.5 V bias), where the redistribution of charge reduces the size of the D_L and enlarges the free carrier concentration. Forward condition is illustrated in **Figure 13(d)**.

Figure 14(a) shows the I-V characteristics for the V-shape SSDs with the reference geometry depicted in **Figure 13(a)** in red solid-line plot where the weak diode-like I-V behavior is appreciated. For this V-shape design, a V_{TH} of ~100 mV and the presence of important current-leakage at reverse breakdown voltage of ~140 mV are presented. Both phenomena are consequence of the short D_L width (along the channel) that is easily filled up when a reverse bias above this voltage is applied. Hence, the D_L extension for the L-shape is larger than the one exhibited by the V-shape SSD, according to **Figures 5(b)** and **13(b)**, respectively. This produces that the V-shape SSD needs a smaller voltage to reach V_{TH} and makes the electrons to flow. Nevertheless, under reverse polarity a leakage current can appear for voltages as low as −0.25 V, reducing the nonlinearity of the device.

The I-V characteristics of V-shape SSDs are sensitive to modifications in their dimensions, as in the case of the L-shape. The performance of the I-V when the channel width, W, is varied is presented in **Figure 14(a)**, while the inset displays the DC behavior when the V leaning angle (α_0) is modified. For this shape, the small D_L between the trenches implies that the diode-like characteristics can be observed only at small W < 45 nm and for thicker size the I-V has a resistor-like behavior. To avoid a reverse current flow and design for a low-V_{TH} V-shape device, to study the relationship between the D_L and α_0 is required. The leaning angle controls the number of free carriers that could occupy the N_S. Therefore, $\alpha_0 > 7°$ is translated in a decay of the D_L width, producing low R_V and V_{TH} in conjunction with poor diode-like behavior. Opposite effect is found to narrow V leaning angles [34] as seen in the inset of **Figure 14(a)**.

Figure 14(b) resumed the impact of the geometry parameters that conform the V-shape SSD by the analysis of the $\gamma_{50\Omega}$ framework where the maximum sensitivity for this analysis is less of 2×10^{-3} V^{-1} caused by the fact that the low R_V and N_V reduce drastically γ_0. According to **Figure 14(b)** in this shape, all modifications have an important role defining the DC characteristics, producing that the design of this device to be more sensitive to the 2DEG and heterostructure properties. The

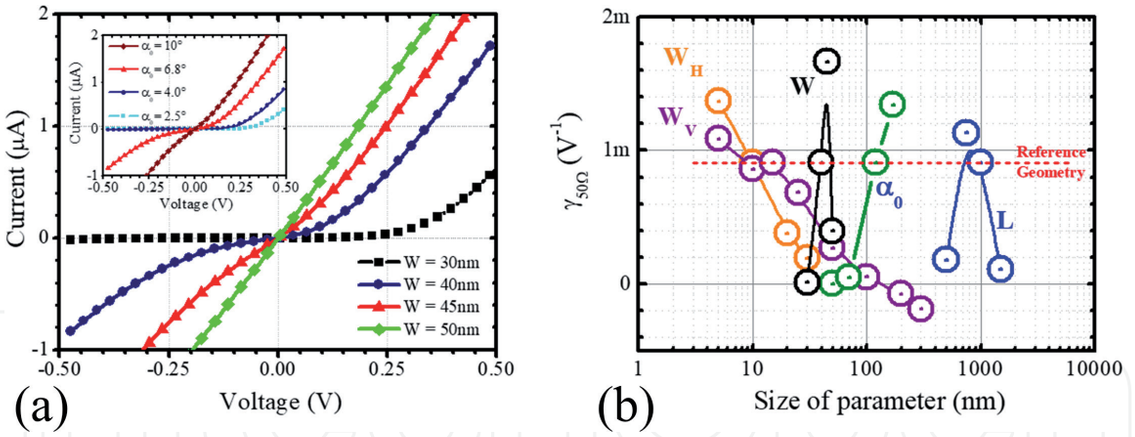

Figure 14.
(a) I-V characteristics of L-shape SSD when the channel width, W, is modified. (b) The inset shows the I-V curves for several leaning angles, α_o.

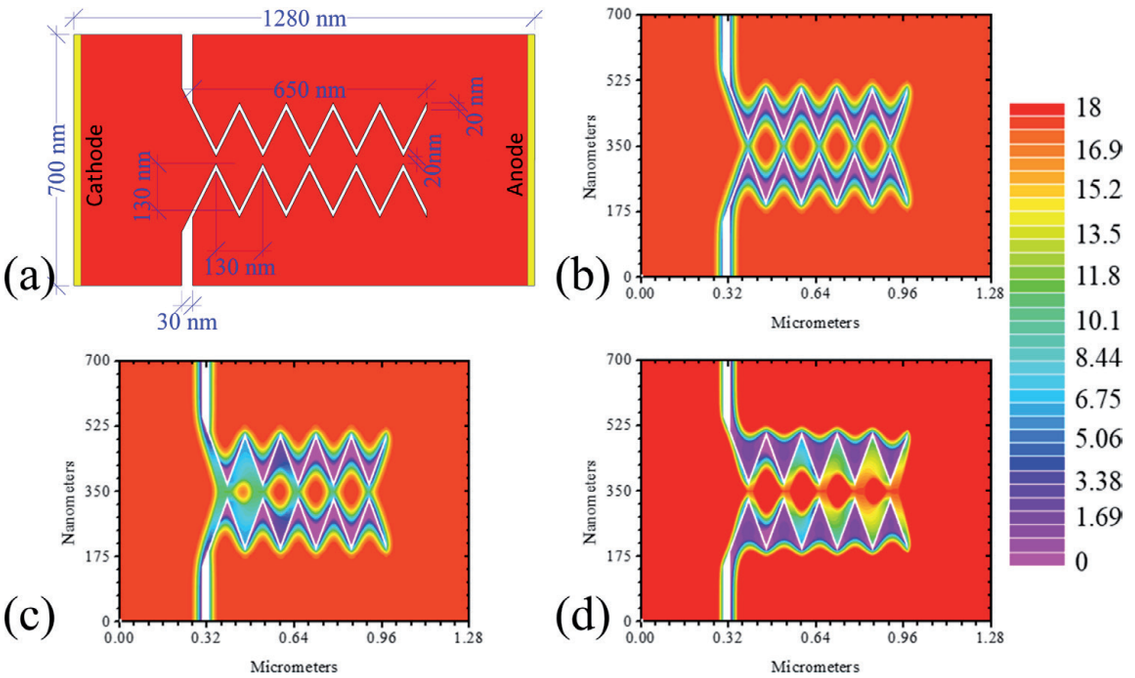

Figure 15.
(a) Two-dimensional scheme of the W-shape SSD where the main geometrical framework is illustrated. Simulation of the W-shape SSD carrier's density for (b) zero bias, (c) reverse bias, and (d) forward bias.

V-shape SSD exhibits poor diode-like characteristics for the 2DEG characteristics used. The fact of the small D_L formed in the channel vortex can be raised if the n_{SS} is strongly elevated or the carrier's concentration is low. Consequently, the L-shape SSD is useless on this condition, being the V-shape the appropriated choice for these situations.

Rendering to previous results, it is necessary to develop a shape of the SSD device that mixed the good rectifier behavior of the L-shape with the low-D_L extension of the V-shape that reduces R_V with the aim to improve the performance of the SSD concept as rectifier. The authors explored the novel SSD shape shown in **Figure 15(a)** labeled as W-shape SSD [40]. In this device, the D_L along the nanochannel has been modified from the completely depleted channel in the L-shape SSD and the less depleted V-shape into a punctual region where the depletion is maximum and easily modified by the electric field applied to electrodes.

For the no-bias situation illustrated in **Figure 15(b)**, the population of electrons inside the nanochannel is enlarged with the vertical distance from the trenches.

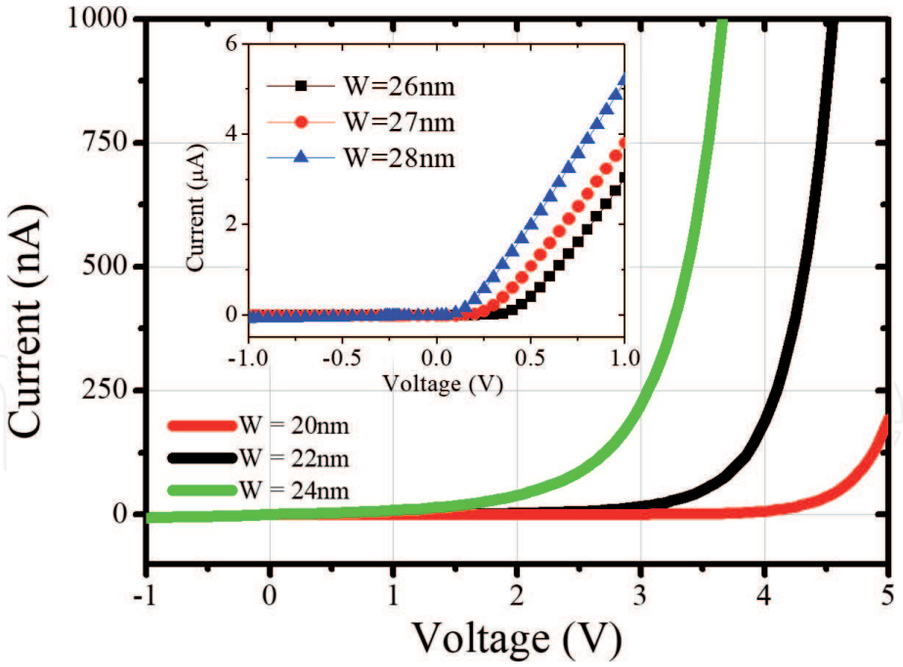

Figure 16.
I-V performance of the W-shape SSD where it is appreciated that the threshold voltage can be modulated by the separation of the grooves.

On the other hand, the electron concentration increases and decreases periodically along the channel, producing an island-like population of electrons with rhombus shape. In this numerical analysis, it is appreciated that the spatial distribution of electrons close to the center of the rhombus is maximum (red color) and it is reduced away to the center of each rhombic electron cluster (cyan color). In this condition the absence of free carriers between the high populated centers of the rhombus can avoid the current flow.

For reverse condition in **Figure 15(c)**, the reduction of the carrier density in the center of the rhombus is obtained, and in the same way, the size of the electron agglomeration is reduced at the left-hand side in contrast with the 0 V case, avoiding free electrons to participate in conduction. When positive voltage is applied to the anode electrode to reduce the D_L, a conducting path close to the chevron corners connects the dots, and a wirelike electron distribution is formed as it is indicated in **Figure 15(d)**, and the current flux can be obtained.

The W-shape SSD current-voltage behavior is dependent on their geometrical dimensions, as in the case of the L- and V-shape devices. Accordingly, the DC performance is optimized by the modification of the shape guidelines, i.e., in the I-V shown in **Figure 16**, the channel width is varied from 20 to 28 nm, being the principal component that determines the DC performance of the SSD as in the case of the L- and V-shape. For the reference geometry with W = 20 nm, the diode-like behavior is present with a negligible negative current, but the V_{TH} is around 4.5 V, undesirable for THz rectification. The slow modification of 1 nm in the channel width modifies strongly the I-V curve in the W-shape SSD.

For instance, the V_{TH} can be tailored by changing the separation of the grooves or the effective channel width from 4.5 to 2.5 V as the channel width is raised from 20 to 24 nm. The inset of **Figure 16** exhibits that when the W-shape SSD is calculated with W > 26 nm, the I-V characteristic behavior turns capable to operate with small power signals owing to the V_{TH} which is near to 0 V. It is important to note the absence of leakage current for reverse bias when the channel width is widened and different behaviors displayed by L- and V-shape designs. The optimization of this device and their performance as rectifier element will be shown in future works.

5. Conclusions

This chapter analyzes the emerging self-switching diode to deal with detection and harvesting of THz radiation from the numerical analysis of their rectifier behavior. The authors have shown the effect of geometry shape and size on the current-voltage performance, finding that the most important values that define the SSD's properties are the channel width and length in conjunction with the trench width for the L-, V-, and W-shape SSDs which are technologically promising by their simplicity in the manufacturing process. We found that the threshold voltage can be tuned to ~0 V, appropriated range for the low power THz signals. The L-shape SSD was analyzed as rectifier element in the rectenna concept where simulations indicate their ability to reach overall efficiencies of ~0.032%, improving the performance of the rectennas based on MIM tunnel barriers for THz applications. The reflection coefficient analysis reveals that one of the problems exhibited by the SSD devices lies in the high-resistance nature of the nanochannel. The reduction of the SSD resistance can be obtained using different shapes which controls the depletion region formed inside the nanochannel. Finally, we conclude that the adequate geometry size and shape of the SSD-based devices must be considered in conjunction with the current development of high-mobility heterostructure and nanolithography process in order to get the ideal rectifier to work in the THz range.

Acknowledgements

The authors acknowledge the financial support from CEMIE-SOL 22, FRC-UASLP, and CONACYT-Mexico through grants INFR-2015-01-255489, CB 2015-257358, PNCPN2014-01-248071, and the Catedras CONACyT (Project No. 44).

Conflict of interest

All authors declare that they have no conflict of interest.

Author details

Irving Eduardo Cortes-Mestizo[1], Edgar Briones[2], Leticia Ithsmel Espinosa-Vega[3] and Victor Hugo Mendez-García[3*]

1 CONACYT-Center for the Innovation and Application of Science and Technology, Autonomous University of San Luis Potosí, San Luis Potosí, Mexico

2 Department of Mathematics and Physics, ITESO Jesuit University of Guadalajara, Tlaquepaque, Mexico

3 Center for the Innovation and Application of Science and Technology, Autonomous University of San Luis Potosí, San Luis Potosí, Mexico

*Address all correspondence to: victor.mendez@uaslp.mx

References

[1] Chamberlain JM. Where optics meets electronics: Recent progress in decreasing the terahertz gap. Philosophical Transactions. Series A, Mathematical, Physical, and Engineering Sciences. 2004;**362**:199-211. DOI: 10.1098/rsta.2003.1312

[2] Maple L, Gow PC, Apostolopoulos V. Simulation of THz generation and propagation from photo-Dember emitters. The Journal of the Optical Society of America B. 2018;**35**(7):1552-1556. DOI: 10.1364/JOSAB.35.001552

[3] Zhao H, Yang L, Zou H, Ma X, Hao Y. Enhancement of negative differential mobility effect in recessed barrier layer AlGaN/GaN HEMT for terahertz applications. IEEE Transactions on Electron Devices. 2019;**66**(3):1236-1242. DOI: 10.1109/TED.2019.2893640

[4] Belkin M, Capasso F. New frontiers in quantum cascade lasers: High performance room temperature terahertz sources. Physica Scripta. 2015;**90**:1-13. DOI: 10.1088/0031-949/90/11/118002

[5] Kojima O, Tarui Y, Shimazu H, Kita T, Majeed A, Ivanov P, et al. Wide frequency tuning of continuous terahertz wave generated by difference frequency mixing under exciton-excitation conditions in a GaAs/AlAs multiple quantum well. Physical Review Applied. 2018;**10**:044035. DOI: 10.1103/PhysRevApplied.10.044035

[6] Ponomarev DS, Lavrukhin DV, Yachmenev AE, Khabibullin RA, Semenikhin IE, Vyurkov VV, et al. Lateral terahertz hot-electron bolometer based on an array of Sn nanothreads in GaAs. Journal of Physics D: Applied Physics. 2018;**51**(13):135101. DOI: 10.1088/1361-6463/aab11d

[7] Norman JC, Jung D, Zhang Z, Wan Y, Liu S, Shang C, et al. A review of high-performance quantum dot lasers on silicon. IEEE Journal of Quantum Electronics. 2019;**55**(2):2000511. DOI: 10.1109/JQE.2019.2901508

[8] Sugaya T. MBE of III-V semiconductors for solar cells. In: Asahi H, Horikoshi Y, editors. Molecular Beam Epitaxy. 1st ed. West Sussex, UK: John Wiley and Sons Ltd; 2019. pp. 265-277

[9] Kuzmik J. Power electronics on InAlN/(In)GaN: Prospect for a record performance. IEEE Electron Device Letters; 2001;**22**:510-512. DOI: 10.1109/55.962646

[10] Daghestani NS, Cataluna MA, Berry G, Ross G, Rose MJ. Terahertz emission from InAs/GaAs quantum dot based photoconductive devices. Applied Physics Letters. 2011;**98**:181107. DOI: 10.1063/1.3586774

[11] Umansky V, Heiblum M. MBE growth of high-mobility 2DEG. In: Henini M, editor. Molecular Beam Epitaxy from Research to Mass Production. 1st ed. Elsevier Inc; 2013. pp. 121-137. DOI: 10.1016/B978-0-12-387839-7.00006-3

[12] Umansky V, de-Picciotto R, Heiblum M. Extremely high-mobility two-dimensional electron gas: Evaluation of scattering mechanisms. Applied Physics Letters. 1997;**71**:683-685. DOI: 10.1063/1.119829

[13] Ajayana J, Nirmal D, Ravichandran T, Mohankumar P, Prajoon P, Arivazhagan L, et al. InP high electron mobility transistors for submillimetre wave and terahertz frequency applications: A review. AEU-International Journal of Electronics and Communications. 2018;**94**:199-214. DOI: 10.1016/j.aeue.2018.07.015

[14] Lüth H. Solid Surfaces, Interfaces and Thin Films. 5th ed. New York,

USA: Springer; 2005. p. 323. DOI: 10.1007/978-3-319-10756-1

[15] Wagner RE, Mandelis A. Intensity dependence of the photoreflectance amplitude in semiconductors. Physical Review B. 1994;**50**:14228-14236. DOI: 10.1103/PhysRevB.50.14228

[16] Cortes-Mestizo IE, Espinosa-Vega LI, Espinoza-Figueroa JA, Cisneros-dela-Rosa A, Eugenio-Lopez E, Mendez-Garcia VH, et al. Determination of the depletion layer width and effects on the formation of double-2DEG in AlGaAs/GaAs heterostructures. Journal of Vacuum Science and Technology B. 2016;**34**:1-6. DOI: 10.1116/1.4942898

[17] Sizov F. THz radiation sensors. Opto-Electronics Review. 2010;**18**:10-36. DOI: 10.2478/s11772-009-0029-4

[18] Bareiss M, Krenz PM, Szakmany GP, Tiwari BN, Kalblein D, Orlov AO, et al. Rectennas revisited. IEEE Transactions on Nanotechnology. 2013;**12**:1144-1150. DOI: 10.1109/TNANO.2013.2281373

[19] Gadalla MN, Abdel-Rahman M, Shamim A. Design, optimization and fabrication of a 28.3 THz nano-rectenna for infrared detection and rectification. Scientific Reports. 2014;4(1):-9. DOI: 10.1038/srep04270

[20] Song AM, Maximov I, Missous M, Seifert W. Diode-like characteristics of nanometer-scale semiconductor channels with a broken symmetry. Physica E: Low-dimensional Systems and Nanostructures. 2004;**21**:1116-1120. DOI: 10.1016/j.physe.2003.11.190

[21] Åberg M, Saijets J, Song A, Prunnila M. Simulation and modeling of self-switching devices. Physica Scripta. 2004;**T114**:123-126. DOI: 10.1088/0031-8949/2004/T114/031

[22] Song AM, Missous M, Omling P, Peaker AR, Samuelson L, Seifert W. Unidirectional electron flow in a nanometer-scale semiconductor channel: A self-switching device. Applied Physics Letters. 2003;**83**: 1881-1883. DOI: 10.1063/1.1606881

[23] Farhi G, Saracco E, Beerens J, Morris D, Charlebois SA, Raskin JP. Electrical characteristics and simulations of self-switching-diodes in SOI technology. Solid-State Electronics. 2007;**51**:1245-1249. DOI: 10.1016/j.sse.2007.07.013

[24] Irshaid YM, Balocco C, Luo Y, Bao P, Brox-Nilsen C, Song AM. Zinc-oxide-based planar nanodiodes operating at 50 MHz. Applied Physics Letters. 2011;**99**:092101. DOI: 10.1063/1.3629995

[25] Kettle J, Perks RM, Hoyle RT. Fabrication of highly transparent self-switching diodes using single layer indium tin oxide. Electronics Letters. 2009;**45**:79-81. DOI: 10.1049/el:20092309

[26] Al-Dirini F, Hossain FM, Nirmalathas A, Skafidas E. All-graphene planar self-switching MISFEDs, metal-insulator-semiconductor field-effect diodes. Scientific Reports. 2014;**4**:1-8. DOI: 10.1038/srep03983

[27] Torres J, Nouvel P, Penot A, Varani L, Sangare P, Grimbert B, et al. Nonlinear nanochannels for room temperature terahertz heterodyne detection. Semiconductor Science and Technology. 2013;**28**:1-6. DOI: 10.1088/0268-1242/28/12/125024

[28] Westlund A, Sangaré P, Ducournau G, Iñiguez-de-la-Torre I, Nilsson PÅ, Gaquière C, et al. Optimization and small-signal modeling of zero-bias InAs self-switching diode detectors. Solid State Electronics. 2015;**104**:79-85. DOI: 10.1016/j.sse.2014.11.014

[29] Balocco C, Kasjoo SR, Lu XF, Zhang LQ, Alimi Y, Winner S, et al. Room-temperature operation of

a unipolar nanodiode at terahertz frequencies. Applied Physics Letters. 2011;**98**:223501. DOI: 10.1063/1.3595414

[30] Mateos J, Vasallo BG, Pardo D, González T. Operation and high-frequency performance of nanoscale unipolar rectifying diodes. Applied Physics Letters. 2005;**86**:212103. DOI: 10.1063/1.1931051

[31] Xu KY, Wang G, Song AM. Electron transport in self-switching nano-diodes. Journal of Computational Electronics. 2007;**6**:59-62. DOI: 10.1007/s10825-006-0048-z

[32] Baraskar AK, Wistey MA, Jain V, Singisetti U, Burek G, Thibeault BJ, et al. Ultralow resistance, nonalloyed ohmic contacts to n-InGaAs. Journal of Vacuum Science and Technology B. 2009;**27**:2036-2039. DOI: 10.1116/1.3182737

[33] Cortes-Mestizo I, Méndez-García VH, Briones J, Pérez-Caro M, Droopad R, McMurtry S, et al. Terahertz harvesting with shape-optimized InAlAs/InGaAs self-switching nanodiodes. AIP Advances. 2015;**5**:117238-117210. DOI: 10.1063/1.4936792

[34] Cortes-Mestizo IE, Briones E, Briones J, Droopad R, Pérez-Caro M, McMurtry S, et al. Study of InAlAs/InGaAs self-switching diodes for energy harvesting applications. Japanese Journal of Applied Physics. 2016;**55**:14304-14307. DOI: 10.7567/JJAP.55.014304

[35] Bean JA, Weeks A, Boreman GD. Performance optimization of antenna-coupled Al/AlO_x/Pt tunnel diode infrared detectors. IEEE Journal of Quantum Electronics. 2011;**47**: 126-135. DOI: 10.1109/JQE.2010.2081971

[36] Gadalla MN, Abdel-Rahman M, Shamim A. Design, optimization and fabrication of a 28.3 THz nano-rectenna for infrared detection and rectification. Scientific Reports. 2014;**4**:4270. DOI: 10.1038/srep04270

[37] Dagenais M, Choi K, Yesilkoy F, Chryssis AN, Peckerar MC. Solar spectrum rectification using nano-antennas and tunneling diodes. Proceedings of SPIE. 2010;**7605**:76050E. DOI: 10.1117/12.845931

[38] Briones E, Cortes-Mestizo IE, Briones J, Droopad R, Espinosa-Vega LI, Vilchis H, et al. Efficiency of broadband terahertz rectennas based on self-switching nanodiodes. Journal of Photonics for Energy. 2017;7(2):025001. DOI: 10.1117/1.JPE.7.025001

[39] Zhang B, He T, Shen T, Hou Y, Hu Y, Zang M, et al. Conjugated polymer-based broadband terahertz wave modulator. Optics Letters. 2014;**39**(21):6110-6113. DOI: 10.1364/OL.39.006110

[40] Balocco C, Song AM, Åberg M, Forchel A, González T, Mateos J, et al. Nano Letters. 2005;**5**:1423-1427. DOI: 10.1021/nl050779g

[41] Cortes-Mestizo IE, Briones E, Belio-Manzano A, Espinosa-Vega LI, Méndez-García VH. W-shape nanodiode controlled by surface states for THz detection. In: 42nd International Conference on Infrared, Millimeter, and Terahertz Waves (IRMMW-THz); 27 Aug.-1 Sept. 2017. Cancun, Mexico: IEEE; 2017. DOI: 10.1109/IRMMW-THz.2017.8067048